Journal of the Mechanics and Physics of Solids 66 (2014) 154–171

Contents lists available at ScienceDirect

Journal of the Mechanics and Physics of Solids

journal homepage: www.elsevier.com/locate/jmps

Modeling a distribution of point defects as misfitting inclusions in stressed solids

W. Cai [a,b,*], R.B. Sills [a,c], D.M. Barnett [a,b], W.D. Nix [b]

[a] Department of Mechanical Engineering, Stanford University, CA 94305, USA
[b] Department of Materials Science and Engineering, Stanford University, CA 94305, USA
[c] Sandia National Laboratories, Livermore, CA 94551, USA

ARTICLE INFO

Article history:
Received 19 September 2013
Received in revised form
6 January 2014
Accepted 9 January 2014
Available online 1 March 2014

Keywords:
Solute
Point defect
Hydrogen
Inclusion
Dislocation

ABSTRACT

The chemical equilibrium distribution of point defects modeled as non-overlapping, spherical inclusions with purely positive dilatational eigenstrain in an isotropically elastic solid is derived. The compressive self-stress inside existing inclusions must be excluded from the stress dependence of the equilibrium concentration of the point defects, because it does no work when a new inclusion is introduced. On the other hand, a tensile image stress field must be included to satisfy the boundary conditions in a finite solid. Through the image stress, existing inclusions promote the introduction of additional inclusions. This is contrary to the prevailing approach in the literature in which the equilibrium point defect concentration depends on a homogenized stress field that includes the compressive self-stress. The shear stress field generated by the equilibrium distribution of such inclusions is proved to be proportional to the pre-existing stress field in the solid, provided that the magnitude of the latter is small, so that a solid containing an equilibrium concentration of point defects can be described by a set of effective elastic constants in the small-stress limit.

1. Introduction

Solid solutions are a ubiquitous feature of metallic systems. They can arise through alloying to enhance mechanical properties, by the introduction of solutes during manufacturing or processing, or via attack by highly permeable contaminants (e.g. hydrogen). The interaction between solutes and other material defects, such as dislocations, can lead to significant changes in the mechanical properties of metals. These interactions can yield desirable effects, as in the case of solid solution strengthening, or undesirable effects, as with hydrogen embrittlement. Possessing a strong theoretical basis for understanding and evaluating the behavior of solid solutions is therefore a necessity for the materials community (Fleischer, 1964; Hirth, 1980; Haasen, 1996).

One key aspect that determines the character of these interactions is the distribution of solutes at chemical equilibrium. Consider a solid containing a set of pre-existing, non-solute defects, such as dislocations or precipitates, which generate a field of internal stresses. Now introduce solutes into the solid. The equilibrium solute distribution depends on the pre-existing stress field. The solutes also generate their own stress fields, whose character depends on the nature of the solutes and the lattice sites they occupy. We will focus on solutes that generate spherically symmetric stress fields, as in the case of octahedral interstitials in face-centered-cubic (FCC) metals. These solute stress fields produce thermodynamic

* Corresponding author.
E-mail addresses: caiwei@stanford.edu (W. Cai), rbsills@stanford.edu (R.B. Sills), barnett@stanford.edu (D.M. Barnett), nix@stanford.edu (W.D. Nix).

http://dx.doi.org/10.1016/j.jmps.2014.01.015
0022-5096

forces on the pre-existing defects, which may, for instance, assist rearrangements of the dislocation structure. If solute diffusion is sufficiently fast, then we may assume the solutes to be in the equilibrium distribution for any instantaneous dislocation configuration. If solute diffusion is not fast enough, then the solute diffusion and dislocation microstructure evolution equations may need to be solved together. Even in this case, the equilibrium solute distribution corresponding to the instantaneous dislocation configuration is still of fundamental importance as it provides a reference state relative to which the solute chemical potential and the driving force for diffusion can be defined.

A common approximation for this problem is to model each point defect as an Eshelby inclusion with a spherical shape and purely dilatational eigenstrain (Eshelby, 1954, 1961) (we will use the terms solute, point defect, and inclusion interchangeably in this work). Often, in order to simplify the analysis both the inclusion and surrounding matrix are treated as elastically isotropic with identical elastic constants. Even though real point defects in crystals introduce additional effects not captured by this simple misfitting inclusion model (modulus effects, electronic effects, etc.), the above approximations provide a valuable starting point for understanding the behavior of point defects and are invoked in this work as well. A significant advantage of this model is that explicit analytical solutions exist for the stress/strain fields and elastic energy of a spherical dilatational inclusion in an infinite solid and, under certain circumstances, in a finite solid. The simplicity of this model makes it easier to expose any potential errors in our intuitive reasoning concerning the solute-defect interaction problem, while such errors can easily be masked in a more complicated model that includes many effects and adjustable parameters.

There have been two predominant approaches presented in the literature for analyzing the problem of a distribution of misfitting inclusions. Both utilize the Eshelby inclusion model to calculate the stress field due to a distribution of point defects, and both use the condition of chemical equilibrium to determine the defect distribution. The difference between the approaches lies in two seemingly small but vital details of the analysis. The first approach, which we will call Approach I, excludes what we will refer to as the *self-stress* of the inclusions, but accounts for the so-called *image stresses* that arise to satisfy the traction-free boundary conditions of the solid. In this paper, we refer to the self-stress as the purely hydrostatic stress found *inside* of each inclusion. The logic behind excluding the self-stress is that because inclusions cannot overlap, the self-stress of existing inclusions is not experienced by the next inclusion to be introduced into the solid, and hence irrelevant to the condition of chemical equilibrium. In contrast, the second approach termed Approach II, ignores the image stress and includes the spatially homogenized self-stress of the inclusions in calculating the equilibrium distribution. Approach II considers the overall stress state of the solid to be a smeared-out homogenization of the stresses both internal and external to the inclusions.

The question of whether Approach I or II is correct has had a long history. The notion of accounting for self-stress was first introduced by Cottrell (1948) and Cottrell and Bilby (1949), who argued that point defects would lessen the hydrostatic tension beneath the glide plane of an edge dislocation and lead to a saturation of the solute concentration, a thesis that requires the self-stress to be included in the equilibrium analysis. But this argument was made before the pioneering work of Eshelby (1954, 1961), who showed that the interaction energy for two dilatational inclusions in an infinite isotropic solid is zero.[1] Based on this result, Thomson (1958) and Hirth and Lothe (1968) excluded the homogenized self-stress field from their analyses. Furthermore, Eshelby (1954) and Hirth and Lothe (1968) pointed out that the presence of a free surface would introduce a position-independent interaction between misfitting defects through the image stresses. So, by the end of the 1960s, after two decades of work focused on discrete atomic point defects on a crystalline lattice, it was widely agreed that the homogenized self-stress field should be excluded and image stresses included in analyzing point defects in stressed solids.[2] We have called this Approach I. But beginning in the early 1970s, in a series of highly cited papers, Larché and Cahn (1973, 1982, 1985) developed a continuum approach to point defect equilibrium that resulted in the re-introduction of the homogenized self-stress and removal of the image stresses. Through this choice they were able to develop an elegant theory that brought the mechanics of point defects into a rigorous thermodynamic framework. The framework developed by Larché and Cahn, which we have called Approach II, has been adopted by others in recent years, including Sofronis (1995), Sofronis and Birnbaum (1995), Chateau et al. (2002), and Delafosse (2012).

With the present paper we wish to conclusively demonstrate that Approach I provides the correct model for understanding the chemo-mechanical equilibrium of solid solution systems. We will present a detailed derivation of the approach and show that in order to have self-consistency, the homogenized self-stress field must be excluded and the images stresses need to be accounted for. Some authors have stated that Approach I is valid only in the limit of dilute solutions (Sofronis, 1995), and we will demonstrate that to the contrary, it is valid both in the dilute limit and beyond. We will then prove analytically that the shear stress induced by a solute atmosphere in equilibrium with the pre-existing stress field is proportional (component by component) to the pre-existing stress, in the limit of small pre-existing stress. As a result, the solid and solutes together behave as a new solid with a set of effective elastic constants, in the limit of small stress. This idea was first presented by Larché and Cahn (1973), but without a proof for the case of non-uniform stress fields. Their expressions were also approximate because the image stresses were ignored. Finally, we will provide a series of numerical results of a solute atmosphere around an edge dislocation to visualize and corroborate our analytic expressions and to contrast the differences between Approaches I and II.

[1] This result is also reproduced in a number of classic texts, such as Khachaturyan (1983) and Mura (1987), and is sometimes referred to as Crum's theorem.

[2] The self-stress is also effectively removed in the continuum theory used by Siems (1970) and Wagner and Horner (1974).

2. Theory

2.1. Fundamental assumptions

We list below the central assumptions upon which all subsequent results are based. For simplicity, we will focus on interstitial solutes that produce spherically symmetric lattice distortion, with hydrogen being our primary interest, even though most of our results can be easily generalized to other cases, e.g. substitutional point defects. Additionally, we mainly consider highly mobile solutes, but the theory holds for solutes of any non-zero mobility as long as the system is given sufficient time to reach equilibrium.

- The solid crystal (i.e. matrix) is modeled as a homogeneous, isotropically elastic medium with shear modulus μ, Poisson's ratio ν, and bulk modulus $K=2\mu(1+\nu)/[3(1-2\nu)]$.
- Each solute is treated as a spherical misfitting inclusion with purely dilational eigenstrain $e^*_{ij}=\overline{e}^*\delta_{ij}$ and the same elastic constants as the matrix. The original lattice volume to be occupied by the inclusion is $V_0=(4\pi/3)r_0^3$.
- The inclusions are only allowed to occupy specific sites in the solid. These allowable sites form a regular lattice with a volume density $c_{\max}=N_s/V$, where N_s is the total number of sites and V is the volume of the solid. $c_{\max}$ is the maximum possible volume density of the solutes. At equilibrium, only a fraction χ of the sites are occupied, so that the volume density of the solutes is $c=\chi c_{\max}$.
- The distance between adjacent sites is greater than $2r_0$, so that no two inclusions can overlap.
- The solutes are sufficiently mobile so that they are always in chemo-mechanical equilibrium with the instantaneous stress field generated by other defects (such as dislocations) and external loads.

If the inclusion is taken out of the matrix and allowed to expand freely, the volume expansion would be $\Delta V\equiv V_0 3\overline{e}^*$. ΔV is often used to represent the extra volume of the solute.

2.2. The distribution of point defects in a stressed solid

We begin by examining the stress field due to a single solute in infinite and finite media, and then consider the behavior of a distribution of inclusions with and without stresses.

2.2.1. A single inclusion in an infinite medium

We will use Eshelby's solution for a misfitting inclusion in an infinite medium. His solution is based on the thought experiment of removing a spherical piece of material from an infinite body, allowing it to expand uniformly by some eigenstrain, and then reinserting the inclusion back into the body. Eshelby (1961) showed if the eigenstrain is hydrostatic then the resulting stress state inside the inclusion is uniform and purely hydrostatic with the form

$$\sigma^{I,\infty}_{ij}=-\frac{4\mu(1+\nu)}{3(1-\nu)}\overline{e}^*\delta_{ij}\quad (r<r_0) \tag{1}$$

where r is the distance from the center of the spherical inclusion to the field point, and δ_{ij} is the Kronecker delta. This will be called *the self-stress* in the following discussions. We can define the pressure corresponding to the self-stress as

$$p^{I,\infty}\equiv-\frac{1}{3}\sigma^{I,\infty}_{ii}=\frac{4\mu(1+\nu)}{3(1-\nu)}\overline{e}^*\quad (r<r_0) \tag{2}$$

where summation over repeated indices is implied. In contrast, outside of the inclusion in the matrix, the stress state is purely deviatoric and varies with position $\mathbf{x}$. It is given by

$$\sigma^{M,\infty}_{ij}(\mathbf{x})=\frac{\mu(1+\nu)}{6\pi(1-\nu)}\Delta V\left(\frac{\delta_{ij}}{r^3}-\frac{3x_ix_j}{r^5}\right)\quad (r>r_0) \tag{3}$$

where $r=|\mathbf{x}|$ and x_i is the i-th component of vector $\mathbf{x}$. The work required to insert the first inclusion in an infinite solid is

$$\Delta W^{\infty}=\frac{1}{2}p^{I,\infty}\Delta V \tag{4}$$

This can be shown by considering a reversible path along which the excess volume of the inclusion varies slowly from 0 to ΔV. The factor of 1/2 appears because the internal pressure varies linearly with the excess volume along this path.

We can apply the same argument to obtain the work done to insert the second inclusion in the infinite solid. In principle, work must be done against the stress field generated by both inclusions. However, since the stress field of the first inclusion is purely deviatoric at the site of the second inclusion, the stress field of the first inclusion produces no work effect on the second inclusion. Hence the work required to create the second (or third, fourth, etc.) inclusion in the infinite solid is the same as that required for the first one, as given in Eq. (4). The required work and hence the final energy of the solid is also

independent of the relative location of the inclusions, as long as they do not overlap. This means that there is no elastic interaction between the inclusions in an infinite medium.[3]

We also point out that the volume expansion of the inclusion embedded in the matrix is

$$\Delta V^{\infty} = \frac{1+\nu}{1-\nu} V_0 \overline{e}^*. \tag{5}$$

Notice that ΔV^{∞} is smaller (for $\nu < 0.5$) than the volume expansion $\Delta V = V_0 3\overline{e}^*$ if the inclusion were taken out of the matrix and allowed to expand freely.

2.2.2. A single inclusion in a finite medium under zero traction

Since all solutes exist in finite bodies, we need to examine how the stress field solution changes in the presence of a free surface, no matter how far away the surface is. Returning to the same inclusion with an initial volume V_0, we now consider it embedded in a finite medium of volume V. Since the medium surface is traction free, the above solution must be modified so that the tractions vanish there. This requires imposing the so-called image stresses on the medium. For an inclusion at the center of a spherical matrix, this image field is uniform and simply given by (Eshelby, 1961)

$$\sigma_{ij}^{\mathrm{img}} = \frac{4\mu(1+\nu)}{9(1-\nu)} \frac{\Delta V}{V} \delta_{ij}. \tag{6}$$

This is a uniform field of positive hydrostatic stress experienced globally throughout the solid.[4] The resulting volume expansion of the matrix is

$$\Delta V^{\mathrm{img}} = V \varepsilon_{ii}^{\mathrm{img}} = \frac{2(1-2\nu)}{1-\nu} V_0 \overline{e}^*. \tag{7}$$

The total volume expansion of the system is that of the inclusion plus that of the matrix:

$$\Delta V^{\infty} + \Delta V^{\mathrm{img}} = V_0 3\overline{e}^* = \Delta V. \tag{8}$$

Thus in the finite solid, the total volume expansion between the isolated inclusion and the inclusion–matrix system is conserved. In other words, the act of inserting the inclusion inside the hole of the matrix, thus creating an internal stress field, does not produce any total volume change, as long as the inclusion and the matrix have the same elastic constants. This is a consequence of Albenga's law (Albenga, 1918/19; Indenbom, 1992) as applied to linear (isotropic and anisotropic) elasticity. We note that Eq. (8) represents the type of "surface effects" that are included in this paper — the ones that persist no matter how far away the surface is, or how large the total volume V is. Other surface effects that depend on the geometry of and proximity to the surface are beyond the scope of this paper.

Finally we define the image pressure as

$$p^{\mathrm{img}} \equiv -\frac{1}{3}\sigma_{ii}^{\mathrm{img}} = -\frac{4\mu(1+\nu)}{9(1-\nu)} \frac{\Delta V}{V} \tag{9}$$

which is a constant throughout the solid.

The work required to insert the first inclusion into a finite solid is

$$\Delta W^{\mathrm{finite}} = \frac{1}{2}\left(p^{\mathrm{I},\infty} + p^{\mathrm{img}}\right)\Delta V = \Delta W^{\infty} + \Delta W^{\mathrm{img}} \tag{10}$$

where ΔW^{img} is the work done against the image stress. Because $p^{\mathrm{img}} < 0$, $\Delta W^{\mathrm{img}} < 0$, so that $\Delta W^{\mathrm{finite}} < \Delta W^{\infty}$. Hence the image stress reduces the energy required to insert an inclusion into a finite solid.

2.2.3. The distribution of inclusions in a finite medium under zero traction

Now we consider the case of a solid containing a three-dimensional periodic array of potential solute sites (e.g. all octahedral sites in an FCC crystal), as illustrated in Fig. 1. Such an arrangement leads to two significant effects: (1) no two solutes can occupy the same solute site and (2) there are a finite number of solute sites that can be occupied, setting a maximum solute concentration limit ($c_{\max}$). We will construct this system by adding more solutes to the system one-by-one up to some quantity N_i. Let us define E_{f} as the energy cost of inserting one solute in an infinite medium (i.e. without considering image stress). If only elastic energy is considered, then E_{f} equals the ΔW^{∞} given in Eq. (4). However, it is sometimes useful to include other energy contributions, such as chemical bonding energy and interfacial energy, in E_{f}. Hence we shall treat E_{f} as an independent parameter in the model. In a finite solid, the work associated with the image stresses needs to be considered. The work associated with external stress and other internal stress fields (e.g. due to

[3] We note that for this conclusion to be true, the misfitting inclusions must have the same elastic constants as the matrix, as is assumed in our model (see Section 2.1).

[4] Strictly speaking, this expression is exact only for an inclusion at the center of a spherical matrix. For inclusions off the center of the matrix, this is an approximation. Eshelby (1954) has also shown that for a solid containing a uniform distribution of solutes, the image stress is uniform at locations further away from the surface than the average distance between nearest solutes. If the deviation of the local solute concentration from a constant is only appreciable at a length scale smaller than λ, then the image stress is very close to be uniform at locations further away from the surface than λ. Nonetheless, the volume average of the image stress over the entire solid is always given by Eq. (6), so that Eqs. (7) and (8) are exact.

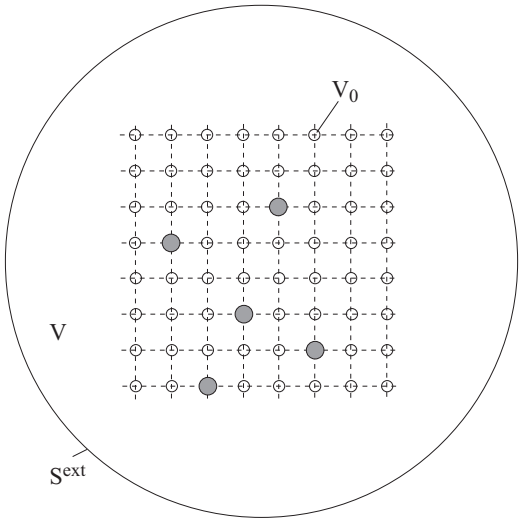

Fig. 1. A schematic showing a solid of volume V and surface S^{ext} containing a periodic array of sites where inclusions can be inserted. Each spherical region to which each inclusion can be inserted has volume V_0. The occupied sites are shown in gray.

dislocations) will be considered in the next section. Note that aside from any image interaction, two solutes *do not directly interact with each other* because they produce purely deviatoric stresses outside themselves in an infinite matrix (see Eq. (3)).

According to Eq. (10), the energy required to insert the first inclusion into the solid is

$$E_{\text{f}}+\frac{1}{2}p^{\text{img}}\Delta V \tag{11}$$

The energy required to insert the second inclusion into the solid is

$$\left(E_{\text{f}}+\frac{1}{2}p^{\text{img}}\Delta V\right)+p^{\text{img}}\Delta V \tag{12}$$

where the last term is the work done against the image stress of the first inclusion. The energy required to insert the $N_{\text{i}}-$th inclusion into the solid is

$$\left(E_{\text{f}}+\frac{1}{2}p^{\text{img}}\Delta V\right)+(N_{\text{i}}-1)p^{\text{img}}\Delta V \tag{13}$$

where the last term is the work done against the image stress of all pre-existing inclusions.

Now, we can express the total enthalpy of the system after having added N_{i} inclusions as follows:

$$\begin{aligned}H(N_{\text{i}}) &= \sum_{n=1}^{N_{\text{i}}}\left[\left(E_{\text{f}}+\frac{1}{2}p^{\text{img}}\Delta V\right)+(n-1)p^{\text{img}}\Delta V\right] = N_{\text{i}}E_{\text{f}}-\frac{4\mu(1+\nu)}{9(1-\nu)}\frac{(\Delta V)^2}{V}\sum_{n=1}^{N_{\text{i}}}\left(n-\frac{1}{2}\right)\\ &= N_{\text{i}}E_{\text{f}}-\frac{2\mu(1+\nu)}{9(1-\nu)}\frac{(\Delta V)^2}{V}N_{\text{i}}^2.\end{aligned} \tag{14}$$

Since there are no external loads, the Gibbs free energy, G, of the solid containing N_{i} inclusions includes the enthalpy, H, and the contribution from the configurational entropy, S. (The vibrational entropy is ignored here.) Thus

$$G(N_{\text{i}}) = H(N_{\text{i}})-TS(N_{\text{i}}) \tag{15}$$

where T is the absolute temperature, and the entropy is

$$S(N_{\text{i}}) = k_{\text{B}}\ln\frac{N_{\text{s}}!}{N_{\text{i}}!(N_{\text{s}}-N_{\text{i}})!} \tag{16}$$

where k_{B} is the Boltzmann constant. The resulting chemical potential of the inclusions is then (using Stirling's formula)

$$\mu_{\text{i}} \equiv \frac{\partial G}{\partial N_{\text{i}}} = E_{\text{f}}-\frac{4\mu(1+\nu)}{9(1-\nu)}\frac{(\Delta V)^2}{V}N_{\text{i}}+k_{\text{B}}T\left[\ln N_{\text{i}}-\ln(N_{\text{s}}-N_{\text{i}})\right]. \tag{17}$$

Let us define the total volume concentration of point defects in the solid under zero pre-existing stress as

$$c_0 = \frac{N_{\text{i},0}}{V} \tag{18}$$

and the fraction of occupied sites as

$$\chi_0 = \frac{N_{i,0}}{N_s} \tag{19}$$

where $c_0 = \chi_0 c_{max}$ and the subscript 0 indicates zero stress. Therefore, if the solid is in equilibrium with a reservoir of inclusions with chemical potential μ_i, the inclusion fraction χ_0 satisfies the following equation:

$$\frac{\chi_0}{1-\chi_0} = \frac{N_i}{N_s - N_i} = \exp\left[-\frac{1}{k_B T}\left(E_f - \frac{4\mu(1+\nu)}{9(1-\nu)}(\Delta V)^2 \frac{N_s}{V}\chi_0 - \mu_i\right)\right] \tag{20}$$

To simplify our notation, we define the following quantity, which appears frequently in our expressions, and has the dimension of energy and is always positive,

$$\xi \equiv \frac{4\mu(1+\nu)}{9(1-\nu)}(\Delta V)^2 \frac{N_s}{V} = \frac{4\mu(1+\nu)}{9(1-\nu)}(\Delta V)^2 c_{max}. \tag{21}$$

Thus we can write Eq. (20) as

$$\chi_0 = \frac{1}{1+\exp\left[\frac{1}{k_B T}\left(E_f - \xi\chi_0 - \mu_i\right)\right]}. \tag{22}$$

This is an implicit equation because χ_0 appears in both sides of the equation. The $-\xi\chi_0$ term on the right-hand side is caused by the (tensile for $\Delta V > 0$) image stress which promotes the introduction of more inclusions into the matrix. If, instead of the image stress, the (compressive) self-stress were (erroneously) included in the analysis, this term would become $+\xi\chi_0$, and would incorrectly predict that the existing inclusions tend to suppress the introduction of more inclusions into the matrix. In order for the self-stress term to appear, the self-stress would have to perform work upon introducing a new inclusion, which would only be possible if the new inclusion were placed *inside* an existing inclusion. Also note that Eq. (22) has the form of a Fermi–Dirac type distribution (Louat, 1956) so that the concentration limit is enforced ($\chi \le 1$) — this is a consequence of the constraint that no more than one inclusion can occupy each solute site.

2.2.4. The distribution of inclusions in a finite medium with inhomogeneous stress

We now consider a finite-sized solid under the influence of an inhomogeneous pre-existing stress field σ_{ij}^d present before the inclusions are introduced. While the superscript d indicates our primary interest in the stress fields produced by dislocations, σ_{ij}^d includes the stress fields generated by other defects as well as by external loads.[5]

To include these pre-existing stresses, we need to consider their energetic contribution. The work done against these stresses upon the introduction of an inclusion is simply

$$\Delta W^d(\mathbf{x}) = -\frac{\sigma_{ii}^d(\mathbf{x})\Delta V}{3}. \tag{23}$$

Notice in this case that because the stress field is heterogeneous, the location of the inclusion affects the amount of work done. This forces us to consider the fraction of inclusions as a field quantity $\chi(\mathbf{x})$. Adding this contribution to the concentration expression, Eq. (22), gives

$$\chi(\mathbf{x}) = \frac{1}{1+\exp\left[\frac{1}{k_B T}\left(E_f - \frac{1}{3}\sigma_{ii}^d(\mathbf{x})\Delta V - \xi\overline{\chi} - \mu_i\right)\right]} \tag{24}$$

where $\overline{\chi} = \langle\chi(\mathbf{x})\rangle$ is the averaged fraction of occupied sites over the entire solid. Noticing that

$$\frac{\chi_0}{1-\chi_0} = \exp\left[-\frac{1}{k_B T}\left(E_f - \xi\chi_0 - \mu_i\right)\right] \tag{25}$$

we can write the inclusion distribution field as

$$\chi(\mathbf{x}) = \left\{1 + \frac{1-\chi_0}{\chi_0}\exp\left[\frac{1}{k_B T}\left(-\frac{1}{3}\sigma_{ii}^d(\mathbf{x})\Delta V - \xi(\overline{\chi} - \chi_0)\right)\right]\right\}^{-1}. \tag{26}$$

Here we have only retained the contribution from the spatially homogeneous part of the image stress. This is a valid approximation in the center region of a large solid, i.e. far away from the surface. To obtain the image stress field exactly would require the solution of a boundary value problem, and is beyond the scope of this paper.[6] Note that the dependence on the chemical potential μ_i is subsumed in the zero stress solute fraction χ_0. Eq. (26) describes the equilibrium distribution of point defects in a solid with arbitrary internal and external stresses at any concentration level. In other words, it remains valid beyond the dilute limit. This result is in direct conflict with the expressions given by Wolfer and Baskes (1985), Sofronis (1995),

[5] Such as those designated by Eshelby as σ_{ij}^A.

[6] In the special case of a spherical solid containing a spherically symmetric solute distribution, i.e. $\chi(\mathbf{x}) = \chi(r)$, where $r = |\mathbf{x}|$, then the image stress is uniform and Eq. (26) is exact.

and Chateau et al. (2002) which include the additional point-wise variant self-stress term and, excluding Wolfer and Baskes (1985), ignore the image stresses.

2.3. The effect of point defects on the stress state of solids

In this section, we will use the above derived solute distribution expressions to analyze how the stress and strain of a solid are modified by the presence of a distribution of misfitting inclusions. Our focus is on shear stresses since they are the only components that exert Peach–Koehler forces on dislocations and cause dislocation motion.[7] We will begin by examining a finite solid under a uniform stress state; this will be done for simplicity and because others have considered this case (Sofronis, 1995). We will then examine a completely general stress field. The general stress state will be assessed by considering a point force in an infinite solid using Green's function of a three-dimensional isotropic solid. We will demonstrate that the effect of a distribution of point defects at equilibrium with any stress state can be accounted for (within the limits of a linearized concentration stress-dependence) with a set of concentration-dependent effective elastic constants. Throughout the derivation, the solid is assumed to be able to exchange solutes with an infinite reservoir, i.e. the solid is an open system.

2.3.1. Uniform stress in a finite body

We now consider a finite-sized solid with no pre-existing internal stress sources (other than the point defects of interest) that is subjected to external loads that produce a uniform stress field, σ_{ij}^{A}. In this case, using Eq. (26) the equilibrium fraction of occupied sites is given by

$$\overline{\chi} = \left\{ 1 + \frac{1-\chi_0}{\chi_0} \exp\left[\frac{1}{k_B T} \left(-\frac{1}{3}\sigma_{ii}^{A}\Delta V - \xi(\overline{\chi}-\chi_0) \right) \right] \right\}^{-1}. \tag{27}$$

This is an implicit equation for $\overline{\chi}$ which has to be solved iteratively. If we take the Taylor expansion of this expression about $\sigma_{ii}^{A}=0$ and neglect higher order terms, we arrive at the approximate linear relationship

$$\overline{\chi}-\chi_0 \approx \chi_0(1-\chi_0)\left[\frac{\sigma_{ii}^{A}\Delta V}{3k_B T} + \frac{\xi}{k_B T}(\overline{\chi}-\chi_0) \right]. \tag{28}$$

Thus we can express the linearized inclusion fraction as

$$\overline{\chi}-\chi_0 \approx \frac{\chi_0(1-\chi_0)\frac{\sigma_{ii}^{A}\Delta V}{k_B T}}{3\left[1-\chi_0(1-\chi_0)\frac{\xi}{k_B T}\right]}. \tag{29}$$

Since we have already shown in Section 2.2.3 that the total volume expansion due to an inclusion in a finite solid is ΔV, Eq. (29) indicates that there is a (dilatational) strain associated with the excess concentration of solutes, in response to the applied stress, of $\varepsilon_{ij}^{c} = \overline{\varepsilon}^{c}\delta_{ij}$, where

$$\overline{\varepsilon}^{c} = (\overline{c}-c_0)\frac{\Delta V}{3} \approx \frac{\chi_0(1-\chi_0)c_{\max}\frac{\sigma_{ii}^{A}(\Delta V)^2}{k_B T}}{9\left[1-\chi_0(1-\chi_0)\frac{\xi}{k_B T}\right]}. \tag{30}$$

The elastic strain in response to the applied stress is $\epsilon_{ij}^{el} = \overline{\epsilon}^{el}\delta_{ij}$, where

$$\overline{\epsilon}^{el} = \frac{\sigma_{ii}^{A}}{9K}. \tag{31}$$

The total dilatational strain is the sum of the contributions from elastic expansion and swelling due to the population of inclusions:

$$\overline{\epsilon}^{tot} = \overline{\epsilon}^{el} + \overline{\varepsilon}^{c}. \tag{32}$$

We may now define an *effective bulk modulus* K_{eff}^{l}

$$K_{eff}^{l} \equiv \frac{\sigma_{ii}^{A}}{9\overline{\epsilon}^{tot}} \tag{33}$$

[7] Hydrostatic stresses can also exert forces on dislocations by the so-called osmotic effects (vacancy production/absorption) — these effects are beyond the scope of the present work, however.

which by inspection is given by

$$\frac{1}{K_{\text{eff}}^{\text{I}}} = \frac{1}{K} + \frac{\chi_0(1-\chi_0)c_{\max}\dfrac{(\Delta V)^2}{k_{\text{B}}T}}{1-\chi_0(1-\chi_0)\dfrac{\xi}{k_{\text{B}}T}}. \tag{34}$$

The superscript I denotes that this is an effective elastic constant based on Approach I (i.e. the correct approach). The shear modulus, μ, is unaffected by the inclusions since they do not impose a net shear strain on the solid. Therefore, we can also define an effective Poisson's ratio as

$$\nu_{\text{eff}}^{\text{I}} \equiv \frac{3K_{\text{eff}}^{\text{I}} - 2\mu}{2(3K_{\text{eff}}^{\text{I}} + \mu)} = 1-(1-\nu)\left[1 - \frac{1+\nu}{2}\,\frac{\xi}{k_{\text{B}}T}\chi_0(1-\chi_0)\right]^{-1} \tag{35}$$

which also leads to

$$\frac{1}{1-\nu_{\text{eff}}^{\text{I}}} = \frac{1}{1-\nu}\left[1 - \frac{1+\nu}{2}\,\frac{\xi}{k_{\text{B}}T}\chi_0(1-\chi_0)\right], \tag{36}$$

an expression that often appears in the stress expressions for edge dislocations. These effective elastic constants are valid as long as the applied stress is small so that the linearized relation, Eq. (28), is accurate.

If we consider the case of a dilute solution, the effective elastic constants simplify further. In this limit, the pre-factor $\chi_0(1-\chi_0)$ (which is due to the non-ideality, i.e. non-Boltzmann character, of the solution) is approximately given by χ_0. Since $\chi_0 \ll 1$ when the solution is dilute, the image term in the denominator of Eq. (29) can also be neglected, because it ultimately leads to a term of the order of χ_0^2. The linearized relationship between $\overline{\chi}$ and σ_{ii}^{A} then simplifies to

$$\overline{\chi} - \chi_0 = \chi_0 \frac{\sigma_{ii}^{\text{A}}\Delta V}{3k_{\text{B}}T} + \mathcal{O}(\chi_0^2). \tag{37}$$

Hence the effective bulk modulus $K_{\text{eff}}^{\text{dilute}}$ is given by

$$\frac{1}{K_{\text{eff}}^{\text{dilute}}} = \frac{1}{K} + c_0\,\frac{(\Delta V)^2}{k_{\text{B}}T}, \tag{38}$$

and the associated effective Poisson's ratio is

$$\nu_{\text{eff}}^{\text{dilute}} \equiv \frac{3K_{\text{eff}}^{\text{dilute}} - 2\mu}{2(3K_{\text{eff}}^{\text{dilute}} + \mu)} = \frac{\nu - \dfrac{c_0(\Delta V)^2}{9k_{\text{B}}T}E}{1 + \dfrac{c_0(\Delta V)^2}{9k_{\text{B}}T}E}, \tag{39}$$

where $E = 2\mu(1+\nu)$ is Young's modulus. These results are the same as those derived by Sofronis (1995), which are here shown to be valid only in the limit of dilute solutions. The effective bulk modulus given by Larché and Cahn (1985) is somewhat in between Eq. (38) and Eq. (34); it maintains the non-ideality pre-factor, $\chi_0(1-\chi_0)$, in the numerator of Eq. (34), but it neglects the image stress term in the denominator.

2.3.2. *Arbitrary internal stress in an infinite body*

We now derive the deviatoric part of the solute stress field in equilibrium with the internal stress field caused by a unit point force applied at the origin along the z-axis in an infinite medium. We will assume the linearized concentration dependence on hydrostatic stress. Since *any* internal stress state can be derived from this solution via a convolution integral, we can use this result to draw conclusions about any arbitrary internal stress state. The elastic Green's function of an infinite, homogeneous isotropic medium is

$$G_{ij} = \frac{1}{8\pi\mu}\left(\delta_{ij}R_{,kk} - \frac{1}{2(1-\nu)}R_{,ij}\right), \tag{40}$$

where $R = \sqrt{x^2+y^2+z^2}$, and a subscript comma denotes partial differentiation, e.g. $R_{,ij} = \partial^2 R/\partial x_i \partial x_j$. Hence the displacement caused by the unit point force along the z-axis is

$$u_i = \frac{1}{8\pi\mu}\left(\delta_{i3}R_{,kk} - \frac{1}{2(1-\nu)}R_{,i3}\right). \tag{41}$$

The resulting displacement gradients are readily obtained as

$$u_{i,j} = \frac{1}{8\pi\mu}\left(\delta_{i3}R_{,kkj} - \frac{1}{2(1-\nu)}R_{,ij3}\right) \tag{42}$$

$$u_{k,k} = \frac{1-2\nu}{16\pi\mu(1-\nu)}R_{,kk3} \tag{43}$$

which then allows us to determine the stress field with

$$\sigma_{ij} = \lambda\delta_{ij}u_{k,k} + \mu(u_{i,j} + u_{j,i}) \tag{44}$$

where $\lambda = 2\mu\nu/(1-2\nu)$ is the Lamé constant. More explicitly, we can write

$$\sigma_{ij} = \frac{1}{8\pi}\left[\delta_{i3}R_{,kkj} + \delta_{j3}R_{,kki} + \frac{\nu}{1-\nu}\delta_{ij}R_{,kk3} - \frac{1}{1-\nu}R_{,ij3}\right]. \tag{45}$$

It can be readily shown that the hydrostatic stress is

$$\sigma_{kk} = \frac{2\mu(1+\nu)}{1-2\nu}u_{k,k} = \frac{1+\nu}{8\pi(1-\nu)}R_{,kk3} \tag{46}$$

and the deviatoric stress is

$$\tilde{\sigma}_{ij} \equiv \sigma_{ij} - \frac{1}{3}\sigma_{kk}\delta_{ij} = \frac{1}{8\pi}\left[\delta_{i3}R_{,kkj} + \delta_{j3}R_{,kki} - \frac{2}{3}\delta_{ij}R_{,kk3}\right] - \frac{1}{8\pi(1-\nu)}\left[R_{,ij3} - \frac{1}{3}\delta_{ij}R_{,kk3}\right]. \tag{47}$$

Since the medium is infinite, the image term is zero, so that the linearized solute distribution change due to the hydrostatic stress field is

$$\chi - \chi_0 = \chi_0(1-\chi_0)\frac{\sigma_{kk}\Delta V}{3k_BT} = \frac{1+\nu}{24\pi(1-\nu)}\frac{\Delta V}{k_BT}\chi_0(1-\chi_0)R_{,kk3}. \tag{48}$$

The deviatoric stress field resulting from this solute cloud can be obtained by invoking the Papkovich–Neuber scalar potential (see Appendix A), B_0, which must satisfy the following Poisson equation:

$$\nabla^2 B_0 = -4\bar{e}^*(1+\nu)(c-c_0)V_0 = -\frac{1+\nu}{8\pi\mu}\frac{\xi}{k_BT}\chi_0(1-\chi_0)R_{,kk3}. \tag{49}$$

This clearly reduces to

$$B_0 = -\frac{1+\nu}{8\pi\mu}\frac{\xi}{k_BT}\chi_0(1-\chi_0)\frac{\partial R}{\partial z}. \tag{50}$$

The deviatoric part of the stress from the distribution of solutes can then be obtained as (see Appendix A)

$$\tilde{\sigma}^c_{ij} = -\frac{\mu}{2(1-\nu)}\left(B_{0,ij} - \frac{1}{3}B_{0,kk}\delta_{ij}\right) = \frac{1+\nu}{16\pi(1-\nu)}\frac{\xi}{k_BT}\chi_0(1-\chi_0)\left[R_{,ij3} - \frac{1}{3}\delta_{ij}R_{,kk3}\right]. \tag{51}$$

The superscript c denotes that this is the *coherency stress field* due to the solutes. Comparing this with Eq. (47), we observe that σ^c_{ij} is proportional to the term in $\tilde{\sigma}_{ij}$ that contains the factor $1/(1-\nu)$. Therefore, the net deviatoric stress (point force plus equilibrated solute cloud) is

$$\begin{aligned}\tilde{\sigma}_{ij} + \tilde{\sigma}^c_{ij} &= \frac{1}{8\pi}\left[\delta_{i3}R_{,kkj} + \delta_{j3}R_{,kki} - \frac{2}{3}\delta_{ij}R_{,kk3}\right] - \frac{1}{8\pi(1-\nu)}\left[R_{,ij3} - \frac{1}{3}\delta_{ij}R_{,kk3}\right] \\ &\quad + \frac{1}{8\pi(1-\nu)}\frac{1+\nu}{2}\frac{\xi}{k_BT}\chi_0(1-\chi_0)\left[R_{,ij3} - \frac{1}{3}\delta_{ij}R_{,kk3}\right] \\ &= \frac{1}{8\pi}\left[\delta_{i3}R_{,kkj} + \delta_{j3}R_{,kki} - \frac{2}{3}\delta_{ij}R_{,kk3}\right] - \frac{1}{8\pi(1-\nu^I_{\text{eff}})}\left[R_{,ij3} - \frac{1}{3}\delta_{ij}R_{,kk3}\right]\end{aligned} \tag{52}$$

Thus, we conclude that the deviatoric stress of an equilibrium distribution of solutes in any stress state can be accounted for with the effective Poisson's ratio using Approach I, Eq. (36).

Note that in this example we are considering an infinite medium where no image stresses are present. And yet, the effective elastic constants derived here match exactly those we found by considering a finite medium including image stress in the previous section. This result is a reflection of the self-consistency of Approach I.

In the above we have referred only to the deviatoric portion of the coherency stress field. The reader should keep in mind that when sampling only regions external to the inclusions, as other inclusions do when diffusing to their equilibrium positions, this is actually the entire coherency stress field, i.e. $\sigma^c_{ij} = \tilde{\sigma}^c_{ij}$. If we instead utilized a smeared-out continuum approach, as in Larché and Cahn (1985), then the homogenized stress field also includes the hydrostatic part of the coherency stress, which is,

$$\sigma^c_{kk} = -\frac{\xi}{k_BT}\chi_0(1-\chi_0)\frac{1+\nu}{8\pi(1-\nu)}R_{,kk3} = -\frac{\xi}{k_BT}\chi_0(1-\chi_0)\sigma_{kk} \tag{53}$$

Note that this stress is proportional to the pre-existing hydrostatic stress σ_{kk} given in Eq. (46). Furthermore, it is exactly the change in σ_{kk} if ν were replaced by ν^I_{eff}.[8]

[8] However, it is important to exclude this σ^c_{kk}, i.e. the homogenized self-stress, from the equilibrium distribution field of solutes, such as in Eq. (26).

3. Numerical results

3.1. Equilibrium solute distribution around an edge dislocation

We first examine the equilibrium solute distribution around an infinitely long, straight edge dislocation in an infinite medium. Physically, we can consider the dislocation at the center of a solid cylinder with a radius R much larger than the region of interest around the dislocation. The change of average solute concentration $\overline{\chi}$ from χ_0 induced by the dislocation vanishes as R goes to infinity. This is the infinite medium limit in which we do not need to consider the image stress[9]. We will use this example to visualize the differences in the predictions between Approach I and Approach II. The material parameters correspond to hydrogen interstitials occupying interstitial sites of the FCC metal palladium (Pd): $\mu=46$ GPa, $\nu=0.385$, $b=2.75$ Å, and $\Delta V/\Omega=0.186$, where $\Omega=14.72\text{Å}^3$ is the volume per Pd atom.

We consider an edge dislocation along the z-axis, with the extra half plane pointing in the $+y$ direction. The Burgers vector points in the x-direction when the sense vector is in the z-direction. The stress field of this dislocation is given in Eq. (B.1). The equilibrium hydrogen fraction depends only on the hydrostatic stress field of the dislocation given in Eq. (B.2). The equilibrium hydrogen fraction field, $\chi(x,y)$, predicted by Approach I can be computed using Eq. (26), with $\overline{\chi}-\chi_0=0$ in this example since we are dealing with an infinite medium. In other words, the correct hydrogen fraction field is

$$\chi^{\mathrm{I}}(x,y)=\left\{1+\frac{1-\chi_0}{\chi_0}\exp\left[\frac{1}{k_{\mathrm{B}}T}\left(-\frac{1}{3}\sigma^{\mathrm{d}}_{ii}(x,y)\Delta V\right)\right]\right\}^{-1}. \tag{54}$$

If Approach II is used instead, then the hydrogen fraction can be computed using the following (incorrect) expression:

$$\chi^{\mathrm{II}}(x,y)=\left\{1+\frac{1-\chi_0}{\chi_0}\exp\left[\frac{1}{k_{\mathrm{B}}T}\left(-\frac{1}{3}\sigma^{\mathrm{d}}_{ii}(x,y)\Delta V+\xi\left(\chi^{\mathrm{II}}(x,y)-\chi_0\right)\right)\right]\right\}^{-1} \tag{55}$$

which is an implicit expression that has to be solved iteratively for every point (x, y).

Fig. 2 shows the $\chi(x,y)$ fields using Approach I (left) and Approach II (right), for zero-stress fractions of (a) $\chi_0=0.01$ and (b) $\chi_0=0.1$. The two values of χ_0 correspond to different chemical potentials μ_{i} of the solutes. It should be noted that the calculations with $\chi_0=0.1$ are for illustration purposes only, since palladium undergoes a phase change at hydrogen concentrations that large at room temperature.

It can be seen that Approach I predicts more hydrogen accumulation beneath the glide plane of the edge dislocation than Approach II does. This is because Approach II incorrectly includes the solute self-stress, which provides a negative feedback to reduce solute accumulation. The difference between the Approach I and Approach II increases with increasing background hydrogen fraction, χ_0.

Fig. 3(a) plots the excess number of solute atoms per unit length around the dislocation, i.e. N/L in the notation of Hirth and Lothe (1968), within a cylinder of radius R, caused by the pressure field of the dislocation. The circles are data obtained by numerically integrating $c(x,y)-c_0$ (from Approach I) over circular areas of radius R. The data agree very well with the analytic expression

$$\frac{N}{L}\approx\frac{\pi\beta^2c_0}{2k_{\mathrm{B}}^2T^2}(1-\chi_0)(1-2\chi_0)\ln\frac{R}{r_c} \tag{56}$$

where

$$\beta=\frac{\mu b(1+\nu)}{3\pi(1-\nu)}\Delta V \tag{57}$$

and r_c is treated as a fitting parameter here. The logarithmic dependence shown in Eq. (56) is consistent with Hirth and Lothe (1968). The only difference is in the factor of $(1-\chi_0)(1-2\chi_0)$ in Eq. (56), which is caused by our use of the Fermi–Dirac distribution, instead of the Boltzmann distribution. The logarithmic divergence of N/L with R indicates that the solute atmosphere is not localized around the dislocation center.

Fig. 3(b) plots the excess number of solute atoms in the domain $y<0$ where $\chi>\chi_0$, i.e. N^+/L, within a half-cylinder of radius R. The numerical data agree very well with the analytic expression

$$\frac{N^+}{L}\approx\frac{2c_0\beta}{k_{\mathrm{B}}T}R+d \tag{58}$$

where d is treated as a fitting parameter here. Eq. (58) indicates that the total excess solute accumulated within a semicircular region below the glide plane increases linearly with radius R. The total depletion of solute, i.e. N^-/L (not shown), within a semicircular region above the glide plane also increases linearly with radius R, similar to Eq. (58). The net accumulation of solute in a circular region of radius R, shown in Fig. 3(a), is the accumulation below the glide plane minus the depletion above the glide plane, i.e. $N/L=N^+/L-N^-/L$.

[9] However, the image stress cannot be ignored if the solid contains a finite density of dislocations as R goes to infinity.

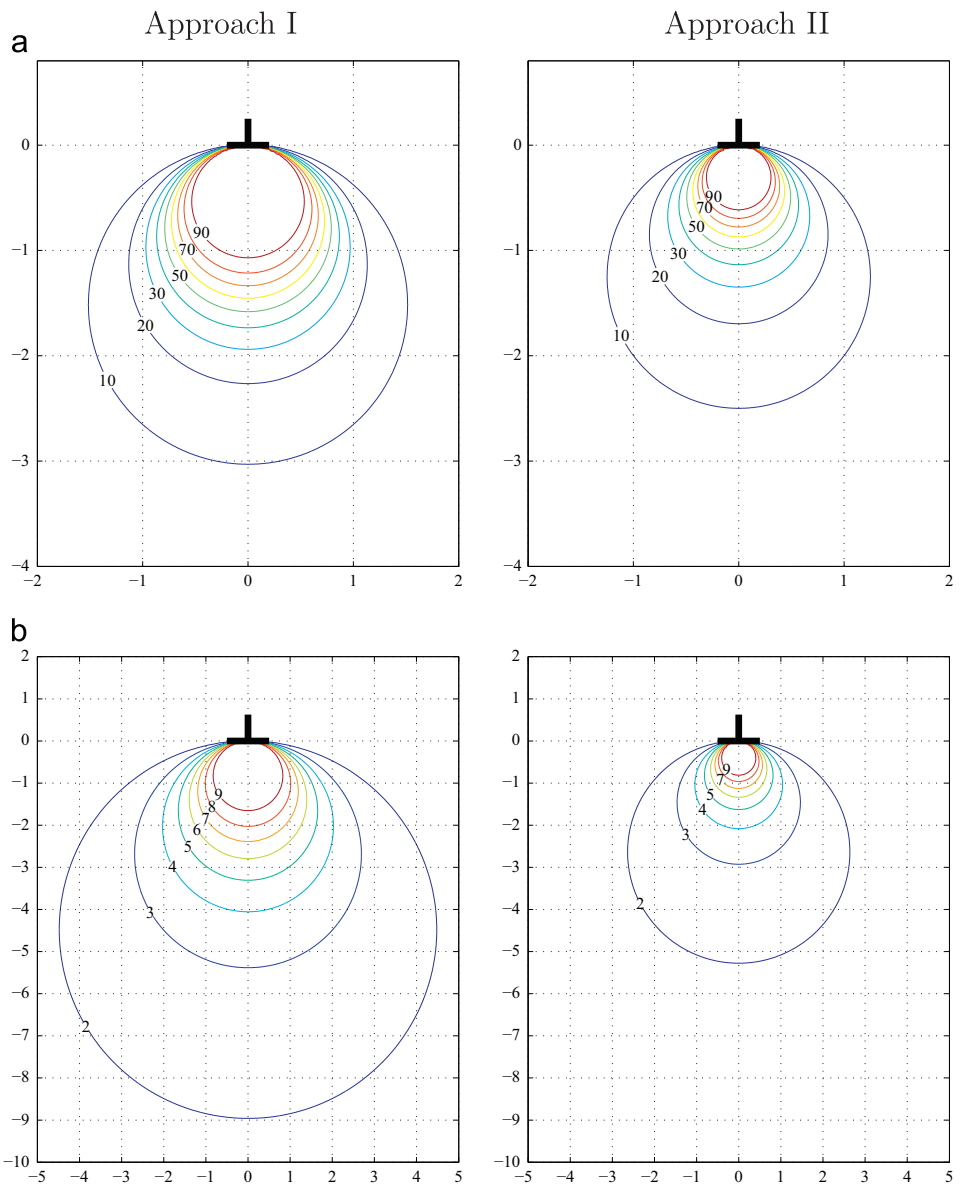

Fig. 2. Distribution of solutes, χ/χ_0, around an edge dislocation in palladium at 300 K with (a) $\chi_0 = 0.01$ and (b) 0.1. Left plots are the results using Approach I and right plots using Approach II. The corresponding values of χ/χ_0 are listed next to the contour lines. Axes are in units of Burgers vectors. Note that the axis scales are different between (a) and (b).

3.2. Solute coherency stress around an edge dislocation

We now compute the coherency stresses due to the equilibrium distribution of solutes around the edge dislocation. The coherency stresses σ^c_{ij} are calculated by convolving the inhomogeneous part of the dilatation density field, $[\chi(x,y)-\chi_0]c_{\max}\Delta V$, with the stress field of a line of unit dilatation, $\sigma^{\text{dila}}_{ij}$, given in Eq. (C.4), i.e.,

$$\sigma^c_{ij}(x,y) = \int_{-\infty}^{\infty}\int_{-\infty}^{\infty} [\chi(x',y')-\chi_0]\, c_{\max}\Delta V \sigma^{\text{dila}}_{ij}(x-x',y-y')\, \mathrm{d}x'\, \mathrm{d}y'. \tag{59}$$

Here we are only interested in the shear stress components of the coherency stress, and for this 2D problem, the two independent shear stress components are: σ^c_{xy} and $(\sigma^c_{xx}-\sigma^c_{yy})$.

The integral of Eq. (59) was evaluated numerically, using the adaptive quadrature function `quad2d` in Matlab. The limits of the integration were truncated at $\pm 10^5 b$, so that every field point (x, y) had stress contributions from a domain of solute concentrations of the same size. The use of adaptive quadrature does not require a pre-specified mesh grid, nor the approximation that solute density is piecewise uniform. Hence the method used here is more accurate than the "constant

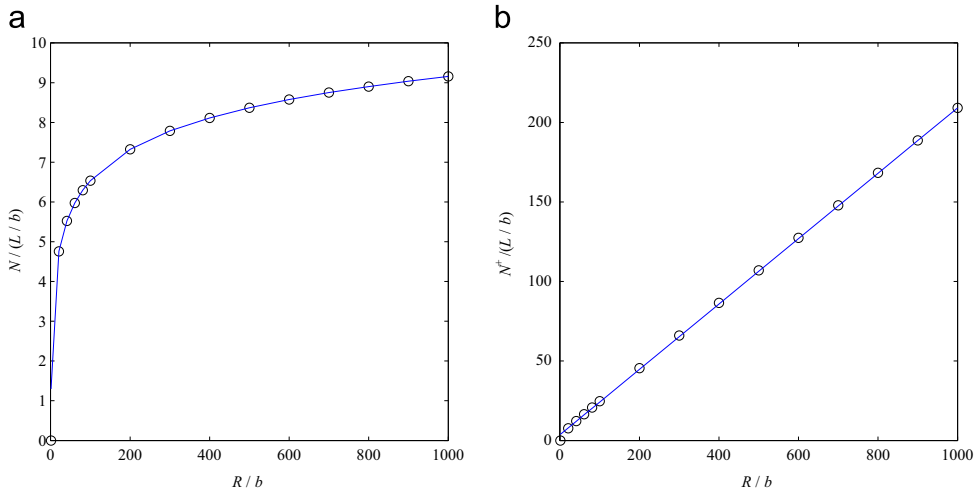

Fig. 3. (a) The total number of excess solutes around the dislocation within a cylinder of radius R per unit length. (b) The total number of excess solutes below the dislocation glide plane around the dislocation within a half-cylinder of radius R per unit length. The circles correspond to numerical data and the lines correspond analytic expressions (see text).

concentration" approach used in Chateau et al. (2002), especially for stress contributions from regions near each field point and those near the dislocation center, where the integrand varies rapidly.

Fig. 4 presents the coherency shear stress σ_{xy} and $\sigma_{xx}-\sigma_{yy}$ results using Approaches I (circles) and II (triangles) along radial lines at angles of $\theta=0^\circ$ and $\theta=45^\circ$ relative to the positive x-axis, for the case of $\chi_0=0.01$. The stress field of the edge dislocation itself, σ_{ij}^{d}, is also plotted as a solid line, which is a straight line here due to its $1/r$ dependence. Notice that $(\sigma_{xx}^{\mathrm{d}}-\sigma_{yy}^{\mathrm{d}})=0$ along $\theta=0^\circ$, while $\sigma_{xy}^{\mathrm{d}}=0$ along $\theta=45^\circ$.

We can see that at distances greater than $10b$ from the dislocation center, the solute coherency shear stresses become proportional to the dislocation stress, i.e. they either develop a $1/r$ dependence or become zero. This is the region where the linearized solute concentration theory becomes valid, and where the solid plus the solutes behave as a new solid with an effective Poisson's ratio ν_{eff}. The coherency shear stresses predicted by the linearized theory are

$$\sigma_{xy}^{\mathrm{c,lin}}=\left[\frac{1}{(1-\nu_{\mathrm{eff}})}-\frac{1}{(1-\nu)}\right]\frac{\mu b}{2\pi}\frac{x(x^2-y^2)}{(x^2+y^2)^2}$$
$$\sigma_{xx}^{\mathrm{c,lin}}-\sigma_{yy}^{\mathrm{c,lin}}=\left[\frac{1}{(1-\nu_{\mathrm{eff}})}-\frac{1}{(1-\nu)}\right]\frac{\mu b}{2\pi}\frac{4x^2y}{(x^2+y^2)^2} \tag{60}$$

where ν_{eff} can be either $\nu_{\mathrm{eff}}^{\mathrm{I}}$, given by Eq. (35) from the full theory (Approach I), or $\nu_{\mathrm{eff}}^{\mathrm{dilute}}$, given by Eq. (39) as an approximation in the dilute limit ($\chi_0 \ll 1$). Even though these results follow from the general proof in 3D (Section 2.3.2), it is instructive to prove them explicitly for the case of solutes in equilibrium with an edge dislocation; this proof is given in Appendix B. It may seem counter-intuitive that the stress field of the solute cloud can have a $1/r$ tail, while the stress field of a single line of dilatation decays as $1/r^2$ at large r. Indeed, if we consider a hypothetical situation where an edge dislocation is suddenly introduced in a solid with an initially uniform solute concentration, then, in the short term, solute diffusion is most pronounced near the dislocation center, from the region above the slip plane to the region below the slip plane. This creates a dilatation dipole (Hirth, 2013), which has a stress field that decays as $1/r^3$. However, after sufficient time is given for the solutes to reach their equilibrium distribution, both the solute density field and the solute stress field develop a $1/r$ tail.

The lines representing the predictions based on $\nu_{\mathrm{eff}}^{\mathrm{I}}$ are almost indistinguishable from those based on $\nu_{\mathrm{eff}}^{\mathrm{dilute}}$, indicating that the dilute limit approximation works well for the present case of $\chi_0=0.01$.

Eqs. (60) and (B.13) show that, far away from the dislocation center, the shear stress of the dislocation plus that of the solute can be quickly obtained by substituting $\nu\to\nu_{\mathrm{eff}}$ in the original shear stress expression of the dislocation. However, caution must be exercised in interpreting the solid + solute system as a new solid with an effective Poisson's ratio ν_{eff}. In particular, the hydrostatic stress field σ_{ii}^{d} that enters Eq. (54) to determine the equilibrium solute fraction must be the original dislocation stress field, i.e. using ν instead of ν_{eff}. For example, it was a mistake in Eq. (5.19) of Larché and Cahn (1985) to use ν^* (which is equivalent to our ν_{eff}) instead of ν to determine the solute concentration. It is for this reason that we have considered the approach of Larché and Cahn as Approach II.

Near the dislocation center ($r<10b$), the actual shear stresses from the solute distribution deviate from the $1/r$ shape predicted by the linearized theory. It is also in this region that the predictions from Approach I and those from Approach II differ clearly from each other. The deviation from the linearized theory is expected because the linearized theory is only valid regions experiencing low stress, which is clearly not the case near the dislocation center. Part of this deviation can be accounted for as a net accumulation of solutes near the dislocation core. A first order approximation of the additional shear

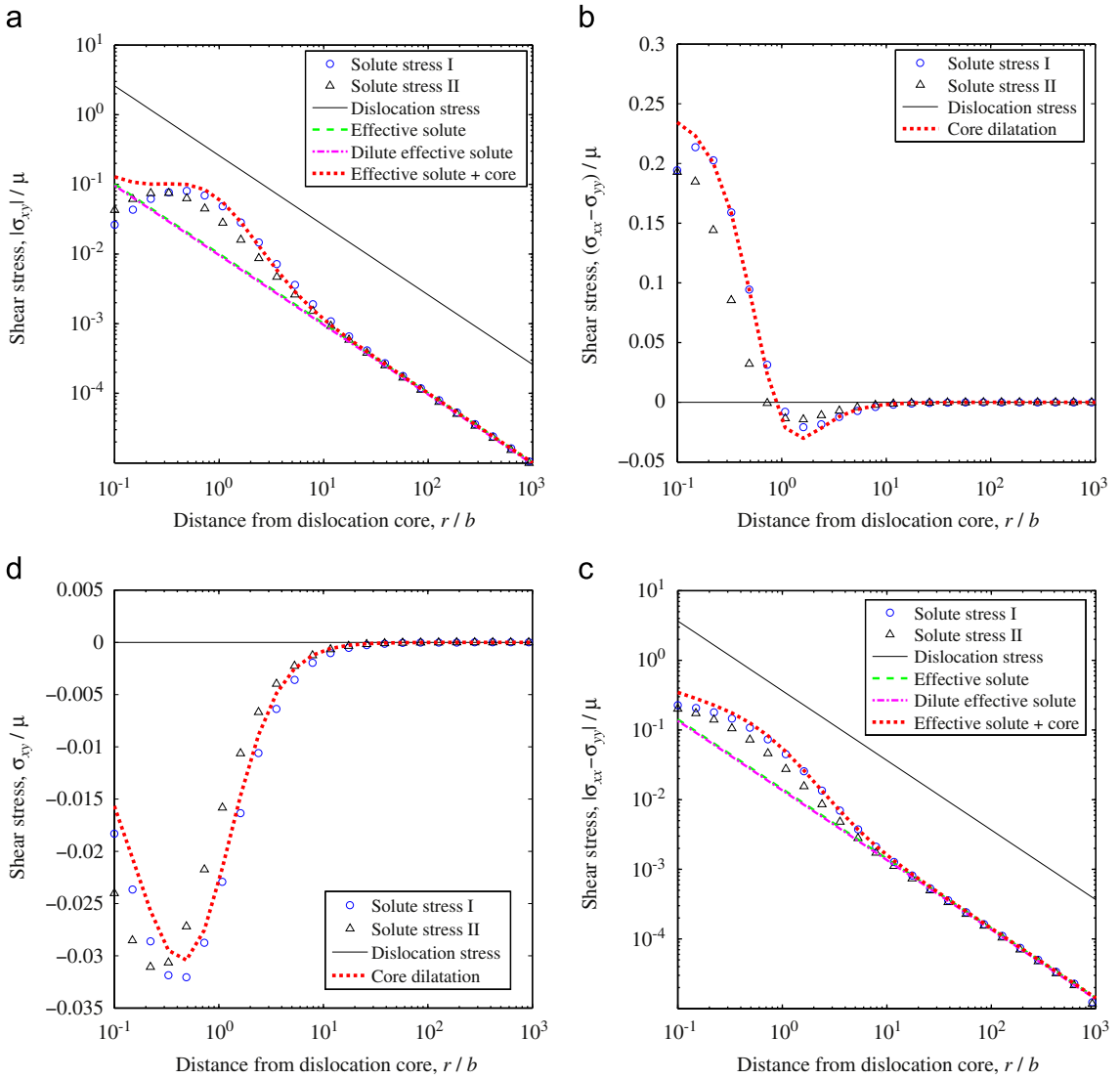

Fig. 4. Shear stress fields (a,c) σ_{xy} and (b,d) $\sigma_{xx}-\sigma_{yy}$ around an edge dislocation in an infinite medium along radial lines at (a,b) 0 ° and (c,d) 45 ° relative to the positive x-axis with $\chi_0 = 0.01$. Shown are the dislocation stresses (solid lines), solute stresses using Approach I (○) and Approach II (△), predicted solute stresses using $\nu^{\mathrm{I}}_{\mathrm{eff}}$ (dashed lines) and $\nu^{\mathrm{dilute}}_{\mathrm{eff}}$ (dot-dashed lines), and solute stresses using $\nu^{\mathrm{I}}_{\mathrm{eff}}$ plus stresses due to a line of dilatation at the dislocation core using a core dilatation radius of $r_{\mathrm{d}} = b$ (dotted lines). Note that the solute stresses in (a) and (d) are negative.

stresses near the core is to treat the excess of solutes there as a lumped line of dilatation. To investigate such a model, we have calculated the stress fields due to lines of dilatation based on a circular region of radius r_{d} centered at r_{d} below the origin. The region has the same shape and relative position to the dislocation as the contour lines shown in Fig. 2, while its size (i.e. radius r_{d}) is chosen empirically. All the lines of dilatation inside this region together are represented by a concentrated line of dilatation, whose strength is the integral of the dilatation strength and whose position is the centroid of the distribution within this circular region. Fig. 4 shows the resulting lumped core dilatation stress field added to the exact effective elastic prediction (short-dashed lines) with $r_{\mathrm{d}} = b$, which was selected based on goodness of fit. The lumped model reproduces the actual solute stress field (Approach I) very well.

4. Conclusions

The main purpose of this paper is to clarify a controversy in the literature concerning how the equilibrium distribution of solutes should depend on the stress field. To ensure that the most important point stands out clearly and unobstructed by unnecessary details, we have considered a simple model in which every solute atom is equivalent to a spherical inclusion with purely dilatational eigenstrain. The matrix and the solutes are modeled as isotropic elastic media with identical elastic constants.

The central point of the controversy is about whether the compressive self-stress inside each inclusion should be included in the expression for the equilibrium distribution of solutes. In Approach I, the compressive self-stress is excluded from consideration, based on the fact that it is never experienced by the next inclusion to be introduced into the solid. Furthermore, when a finite solid is considered, Approach I takes into account the tensile image stress field that is needed to satisfy the traction-free boundary condition. In Approach II, exactly the opposite treatment is used: the compressive self-stress is included, and the tensile image stress is excluded.

We have provided explicit derivations and physical explanations that conclusively prove that Approach I is correct, and Approach II is incorrect. The differences between the predictions from Approach I and Approach II are illustrated for hydrogen solutes surrounding an edge dislocation. The main difference is in the distribution near the dislocation core. Far away from the dislocation core, both approaches predict a solute coherency shear stress field that has the same $1/r$ tail as the dislocation stress field itself. The $1/r$ tail can be described by a change of Poisson's ratio to an effective Poisson's ratio. However, in the usual case of a low back-ground solute concentration χ_0, this effect is very small, and the difference between the two approaches is even smaller and hardly noticeable.

The difference between Approach I and Approach II is perhaps best illustrated by considering the equilibrium distribution of solutes in an inhomogeneous internal stress field in the zero temperature limit. According to Approach I, Eq. (24), in the limit of $T \to 0$, the local solute fraction is 1 at regions where the local tensile stress is sufficiently large so that the sum of all terms inside the round bracket is negative. In these regions, all available solute sites are occupied, so that the local concentration equals $c_{\max}$. In all the remaining regions, the local solute fraction is 0. Therefore, Approach I predicts a "binary" distribution scenario in the zero temperature limit, where the local fraction of solutes at every point is either 0 or 1.

On the contrary, in Approach II it is possible to have a smoothly varying solute concentration field in the presence of a smoothly varying internal stress field. This happens when the compressive self-stress from the local solute concentration exactly cancels the local tensile field of the pre-existing internal stress (Chateau et al., 2002). This corresponds to the suggestion in Cottrell (1948) and Cottrell and Bilby (1949) that existing solutes "relax" the local tensile stress field of dislocations. However, as we have shown extensively in this paper, this scenario envisioned by Approach II is erroneous. Solutes do not "relax" the local tensile stress field of dislocations in the sense of reducing the local driving force for solute segregation. On the contrary, if the image stress is taken into account, existing solutes actually produce a tensile stress field in the solid that promotes the incorporation of more solutes.

As emphasized earlier, we have focused our discussions on the simple model of solutes as spherical inclusions with a purely dilatational eigenstrain in an isotropic medium. However, the main conclusion that the self-stress must be excluded (and image stress included) in the equilibrium distribution of solutes *remains true in general*, for example, even if the solutes are modeled as inclusions with shear eigenstrains in anisotropic media. As long as the solute is modeled as an inclusion embedded in a continuum matrix, there is a self-stress "locked-inside" each inclusion. This self-stress may contain both hydrostatic and (in the general case) deviatoric components, but it is *not* experienced by the next inclusion to be introduced into the solid. Hence the self-stress does not enter the equilibrium distribution expression of the solutes. This holds true because, ultimately, solute atoms are discrete entities. Therefore, the error of Approach II illustrates the need to be careful when developing homogenized continuum theories for a collection of discrete objects. Sometimes the *discrete* nature of the objects *persists* even in the equations that describe homogenized fields, such as the equilibrium distribution expression.

Acknowledgments

We wish to thank Dr. J.P. Hirth and Dr. W.G. Wolfer for useful discussions. This work was supported by the U.S. Department of Energy, Office of Basic Energy Sciences, Division of Materials Sciences and Engineering under Award No. DE-SC0010412 (W.C.), and Award No. DE-FG02-04ER46163 (W.D.N.), and by Sandia National Laboratories (R.B.S.). Sandia National Laboratories is a multi-program laboratory managed and operated by Sandia Corporation, a wholly owned subsidiary of Lockheed Martin Corporation, for the U.S. Department of Energy's National Nuclear Security Administration under Contract DE-AC04-94AL85000.

Appendix A. Stress field of dilatational eigenstrain in infinite medium

Here we derive the expressions for the stress field due to a distribution of purely dilatational eigenstrains in an infinite medium, in terms of the scalar potential B_0. The expressions have been used in Wolfer and Baskes (1985), but are derived here for completeness. The derivation also makes it clear that the stress given by these expressions have included the self-stress, which is purely hydrostatic. Therefore, the deviatoric part of these stress expressions does not contain the self-stress.

We start from the equilibrium condition of the stress field σ_{ij} in the absence of body forces,

$$\sigma_{ij,j} = 0. \tag{A.1}$$

In a linear elastic isotropic medium, the stress can be written in terms of the elastic strain $\epsilon^{\mathrm{el}}_{ij}$,

$$\sigma_{ij} = \lambda \epsilon^{\mathrm{el}}_{kk} \delta_{ij} + 2\mu \epsilon^{\mathrm{el}}_{ij} \tag{A.2}$$

where $\lambda = 2\mu\nu/(1-2\nu)$ is Lamé constant. The elastic strain ϵ_{ij}^{el} is the difference between the total strain ϵ_{ij}^{tot} and the eigenstrain e_{ij}^*, and the total strain is defined through the spatial derivatives of the displacement field,

$$\epsilon_{ij}^{tot} = \tfrac{1}{2}\left(u_{i,j}+u_{j,i}\right). \tag{A.3}$$

Therefore, the stress can be written as

$$\sigma_{ij} = \lambda(u_{k,k}-e_{kk}^*)\delta_{ij}+\mu(u_{i,j}+u_{j,i}-2e_{ij}^*). \tag{A.4}$$

Hence the equilibrium condition can be written in terms of the displacement field as

$$(\lambda+\mu)u_{k,ki}+\mu u_{i,kk} = \lambda e_{kk,i}^*+2\mu e_{ik,k}^*. \tag{A.5}$$

Assuming that the eigenstrain field is due to a concentration field $c(\mathbf{x})$ (number per unit volume) of purely dilatational inclusions, we have

$$e_{ij}^* = \frac{\Delta V}{3}\delta_{ij}[c(\mathbf{x})-c_0] \tag{A.6}$$

where ΔV is the excess volume of each inclusion, and c_0 is the uniform background concentration. The equilibrium condition becomes

$$u_{i,kk}+\frac{1}{1-2\nu}u_{k,ki} = \frac{1+\nu}{1-2\nu}\,\frac{2\Delta V}{3}\left[c_i(\mathbf{x})-c_{0,j}\right]. \tag{A.7}$$

In an infinite medium, the solution can be obtained by introducing a scalar potential $B_0(\mathbf{x})$ (Gurtin, 1972) such that

$$u_i = -\frac{1}{4(1-\nu)}B_{0,i}. \tag{A.8}$$

In terms of B_0, the equilibrium condition becomes

$$B_{0,ikk} = -\frac{4\Delta V}{3}(1+\nu)\left[c_i(\mathbf{x})-c_{0,i}\right] \tag{A.9}$$

which is obviously satisfied if

$$\nabla^2 B_0 \equiv B_{0,kk} = -\frac{4\Delta V}{3}(1+\nu)[c(\mathbf{x})-c_0]. \tag{A.10}$$

This is equivalent to Eq. (10) of Wolfer and Baskes (1985). Therefore, the scalar potential B_0 can be obtained from the concentration field by solving Poisson's equation.

After B_0 is determined, the stress field can be obtained from Eq. (A.4), which gives

$$\sigma_{ij}^c = -\frac{\mu}{2(1-\nu)}B_{0,ij}-\frac{2\mu(1+\nu)}{1-\nu}\,\frac{\Delta V}{3}\delta_{ij}[c(\mathbf{x})-c_0]. \tag{A.11}$$

This is equivalent to Eq. (11) of Wolfer and Baskes (1985). Here we have added the superscript c to indicate that it is the coherency stress of the solutes. The stress given in Eq. (A.11) includes the homogenized self-stress inside each inclusion. The hydrostatic part of this stress is

$$\sigma_{kk}^c = -\frac{4\mu(1+\nu)}{1-\nu}\,\frac{\Delta V}{3}[c(\mathbf{x})-c_0] \tag{A.12}$$

which is proportional to the local concentration of inclusions. We emphasize that this stress field is entirely "locked inside" each existing inclusion and not experienced by any new inclusion to be introduced into the matrix. Hence it should not enter the chemical potential of solutes. Since the self-stress is purely hydrostatic, the deviatoric part of the stress field, given below, does not contain the self-stress contribution,

$$\tilde{\sigma}_{ij}^c \equiv \sigma_{ij}^c-\frac{1}{3}\sigma_{kk}^c\delta_{ij} = -\frac{\mu}{2(1-\nu)}\left(B_{0,ij}-\frac{1}{3}B_{0,kk}\delta_{ij}\right). \tag{A.13}$$

Appendix B. Linearized solute coherency stress field around an edge dislocation

Here we give an explicit derivation of the linearized solute coherency stress around an edge dislocation, and prove Eq. (60). Even though Eq. (60) follows from the more general proof in 3D (Section 2.3.2), it is instructive to obtain the explicit expressions for this special case. The following derivation will explicitly show the $1/r$ tail of the coherency stress around the dislocation, and predict an effective Poisson's ratio that is identical to Eq. (35), illustrating the self-consistency of Approach I.

We start with the stress field of an edge dislocation at the origin with Burgers vector along the positive x-axis and sense vector along the positive z-axis (Hirth and Lothe, 1968),

$$\begin{aligned}
\sigma^{\mathrm{d}}_{xx} &= -\frac{\mu b}{2\pi(1-\nu)}\,\frac{y(3x^2+y^2)}{(x^2+y^2)^2}\\
\sigma^{\mathrm{d}}_{yy} &= \frac{\mu b}{2\pi(1-\nu)}\,\frac{y(x^2-y^2)}{(x^2+y^2)^2}\\
\sigma^{\mathrm{d}}_{zz} &= \nu(\sigma_{xx}+\sigma_{yy}) = -\frac{\mu b\nu}{\pi(1-\nu)}\,\frac{y}{x^2+y^2}\\
\sigma^{\mathrm{d}}_{xy} &= \frac{\mu b}{2\pi(1-\nu)}\,\frac{x(x^2-y^2)}{(x^2+y^2)^2}\\
\sigma^{\mathrm{d}}_{xx}(x,y)-\sigma^{\mathrm{d}}_{yy}(x,y) &= -\frac{\mu b}{2\pi(1-\nu)}\,\frac{4x^2y}{(x^2+y^2)^2}.
\end{aligned} \tag{B.1}$$

Hence, the hydrostatic stress field is

$$\frac{1}{3}\sigma^{\mathrm{d}}_{ii} = \frac{1}{3}\left(\sigma^{\mathrm{d}}_{xx}+\sigma^{\mathrm{d}}_{yy}+\sigma^{\mathrm{d}}_{zz}\right) = -\frac{\mu b(1+\nu)}{3\pi(1-\nu)}\frac{y}{x^2+y^2} \tag{B.2}$$

and the linearized concentration field is

$$\begin{aligned}
c-c_0 &= c_{\max}(\chi-\chi_0) = c_0(1-\chi_0)\frac{\sigma^{\mathrm{d}}_{ii}\Delta V}{3k_{\mathrm{B}}T}\\
&= -c_0(1-\chi_0)\frac{\mu b(1+\nu)}{\pi(1-\nu)}\,\frac{y}{x^2+y^2}\,\frac{\Delta V}{3k_{\mathrm{B}}T}.
\end{aligned} \tag{B.3}$$

The stress field of this solute atmosphere can be obtained by integrating the stress contribution from each line of dilatation over the entire domain, as given in Eq. (59). The stress field of a line of dilatation located at the origin is given in Eq. (C.4). For example, the xy component of the shear stress of the solute cloud is

$$\begin{aligned}
\sigma^{\mathrm{c}}_{xy}(x,y) &= \int_{-\infty}^{\infty}\int_{-\infty}^{\infty}\left[-c_0(1-\chi_0)\frac{\mu b(1+\nu)}{\pi(1-\nu)}\frac{y'}{x'^2+y'^2}\,\frac{\Delta V}{3k_{\mathrm{B}}T}\right]\Delta V\left[-\frac{\mu(1+\nu)}{3\pi(1-\nu)}\,\frac{2(x-x')(y-y')}{[(x-x')^2+(y-y')^2]^2}\right]\mathrm{d}x'\,\mathrm{d}y'\\
&= \frac{\mu b(1+\nu)}{2\pi(1-\nu)}\xi\chi_0(1-\chi_0)\int_{-\infty}^{\infty}\int_{-\infty}^{\infty}\frac{1}{\pi}\,\frac{y'}{x'^2+y'^2}\,\frac{(x-x')(y-y')\,\mathrm{d}x'\,\mathrm{d}y'}{[(x-x')^2+(y-y')^2]^2}.
\end{aligned} \tag{B.4}$$

The integral can be carried out analytically to give

$$\sigma^{\mathrm{c}}_{xy}(x,y) = \frac{\mu b(1+\nu)}{2\pi(1-\nu)}\xi\chi_0(1-\chi_0)\left[-\frac{x(x^2-y^2)}{2(x^2+y^2)^2}\right] = -\frac{1+\nu}{2}\,\frac{\xi}{k_{\mathrm{B}}T}\chi_0(1-\chi_0)\sigma^{\mathrm{d}}_{xy}(x,y). \tag{B.5}$$

Similarly, we can show that

$$\sigma^{\mathrm{c}}_{xx}(x,y)-\sigma^{\mathrm{c}}_{yy}(x,y) = \frac{\mu b(1+\nu)}{2\pi(1-\nu)}\xi\chi_0(1-\chi_0)\left[\frac{2x^2y}{(x^2+y^2)^2}\right] = -\frac{1+\nu}{2}\,\frac{\xi}{k_{\mathrm{B}}T}\chi_0(1-\chi_0)\left[\sigma^{\mathrm{d}}_{xx}(x,y)-\sigma^{\mathrm{d}}_{yy}(x,y)\right]. \tag{B.6}$$

This means that the shear stress of the solute cloud is proportional to the original shear stress of the dislocation.

In the following, we give an alternative proof of Eqs. (B.5) and (B.6) using the Papkovich–Neuber scalar potential, which is commonly used in the literature (Wolfer and Baskes, 1985). To find the stress field of this solute atmosphere, we first solve the following Poisson equation for the scalar potential B_0 (see Appendix A),

$$\nabla^2 B_0 = -4\bar{e}^*(1+\nu)(c-c_0)V_0 \tag{B.7}$$

which, using Eq. (B.3), is

$$\nabla^2 B_0 = A\frac{y}{x^2+y^2} \tag{B.8}$$

where

$$A \equiv \frac{(1+\nu)b}{\pi}\,\frac{\xi}{k_{\mathrm{B}}T}\chi_0(1-\chi_0). \tag{B.9}$$

The solution is

$$B_0 = \frac{1}{4}A\left[y\ln(x^2+y^2)-y\right]. \tag{B.10}$$

The deviatoric part of the stress from the solute atmosphere can be obtained from

$$\sigma^{\mathrm{c}}_{xy} = -\frac{\mu}{2(1-\nu)}B_{0,xy}$$

$$\sigma^{c}_{xx}-\sigma^{c}_{yy}=-\frac{\mu}{2(1-\nu)}\left(B_{0,xx}-B_{0,yy}\right) \tag{B.11}$$

which results in

$$\begin{aligned}\sigma^{c}_{xy}&=-\frac{A}{2}\,\frac{\mu}{2(1-\nu)}\,\frac{x(x^2-y^2)}{(x^2+y^2)^2}=-\frac{1+\nu}{2}\,\frac{\xi}{k_BT}\chi_0(1-\chi_0)\sigma^{d}_{xy}\\ \sigma^{c}_{xx}-\sigma^{c}_{yy}&=A\frac{\mu}{2(1-\nu)}\,\frac{2x^2y}{(x^2+y^2)^2}=-\frac{1+\nu}{2}\,\frac{\xi}{k_BT}\chi_0(1-\chi_0)\left(\sigma^{d}_{xx}-\sigma^{d}_{yy}\right).\end{aligned} \tag{B.12}$$

The total shear stress (dislocation + solute) is then

$$\begin{aligned}&\sigma^{d}_{xy}+\sigma^{c}_{xy}=\frac{\mu b}{2\pi(1-\nu)}\,\frac{x(x^2-y^2)}{(x^2+y^2)^2}\left[1-\frac{1+\nu}{2}\,\frac{\xi}{k_BT}\,\chi_0(1-\chi_0)\right]=\frac{\mu b}{2\pi(1-\nu^{I}_{eff})}\,\frac{x(x^2-y^2)}{(x^2+y^2)^2}\\ &\left(\sigma^{d}_{xx}+\sigma^{c}_{xx}\right)-\left(\sigma^{d}_{yy}+\sigma^{c}_{yy}\right)=-\frac{\mu b}{2\pi(1-\nu)}\,\frac{4x^2y}{(x^2+y^2)^2}\left[1-\frac{1+\nu}{2}\,\frac{\xi}{k_BT}\chi_0(1-\chi_0)\right]=\frac{\mu b}{2\pi(1-\nu^{I}_{eff})}\,\frac{4x^2y}{(x^2+y^2)^2}\end{aligned} \tag{B.13}$$

where ν^{I}_{eff} is the same as the one given in Eq. (35). Note that the solute stress field has the opposite sign from the dislocation stress field. In other words, the solute atmosphere reduces the shear stresses of the dislocation.

The hydrostatic part of the coherency stress field, i.e. the homogenized self-stress, can be obtained by combining Eqs. (A.12) and (B.3)

$$\sigma^{c}_{kk}=\frac{4\mu(1+\nu)}{1-\nu}\,\frac{\Delta V}{3}c_{max}\chi_0(1-\chi_0)\frac{\mu b(1+\nu)}{\pi(1-\nu)}\frac{y}{x^2+y^2}\,\frac{\Delta V}{3k_BT}=-\frac{\xi}{k_BT}\chi_0(1-\chi_0)\sigma^{d}_{kk} \tag{B.14}$$

This is consistent with Eq. (53). The hydrostatic part of the coherency stress is the same as the change of the hydrostatic part of the pre-existing stress of the dislocation if ν were to be changed to ν^{I}_{eff}. The homogenized pressure field in the solid is indeed reduced by σ^{c}_{kk}. However, it is important to exclude σ^{c}_{kk}, i.e. the homogenized self stress, from the equilibrium distribution field of solutes, such as in Eq. (26).

Appendix C. Deviatoric stress field of a line of dilatation

Here we give the stress field of a line of dilatation, which is used in the numerical example in Section 3.2. For a concentrated line of dilatation with excess volume ΔV per unit length, we need to first solve for the scalar potential field B_0 from the following equation:

$$\nabla^2 B_0=-\frac{4}{3}\Delta V(1+\nu)\delta^2(\mathbf{x}) \tag{C.1}$$

where $\delta^2(\mathbf{x})$ is the delta function in 2D. Noting that

$$\nabla^2\left(\frac{1}{2\pi}\ln r\right)=\delta^2(\mathbf{x}) \tag{C.2}$$

and letting $\Delta V=1$ to derive expressions for unit dilatation, we have

$$B_0=-\frac{2(1+\nu)}{3\pi}\ln r. \tag{C.3}$$

The deviatoric part of the stress field can be obtained by differentiation as

$$\begin{aligned}\sigma^{dila}_{xy}&=-\frac{\mu}{2(1-\nu)}B_{0,xy}=-\frac{\mu(1+\nu)}{3\pi(1-\nu)}\,\frac{2xy}{(x^2+y^2)^2}\\ \sigma^{dila}_{xx}-\sigma^{dila}_{yy}&=-\frac{\mu}{2(1-\nu)}\left(B_{0,xx}-B_{0,yy}\right)=-\frac{\mu(1+\nu)}{3\pi(1-\nu)}\,\frac{2(x^2-y^2)}{(x^2+y^2)^2}.\end{aligned} \tag{C.4}$$

References

Albenga, G., 1918/19. Sul problema delle coazioni elastiche. Atti Accad. Sci. Torino Cl. Sci. Fis. Mat. Natur. 54, 864–868.
Chateau, J.P., Delafosse, D., Magnin, T., 2002. Numerical simulations of hydrogen-dislocation interactions in fcc stainless steels. Part I: hydrogen-dislocation interactions in bulk crystals. Acta Mater. 50, 1507–1522.
Cottrell, A.H., 1948. Effect of solute atoms on the behaviour of dislocations. Report of a Conference on Strength of Solids. The Physical Society, London.
Cottrell, A.H., Bilby, B.A., 1949. Dislocation theory of yielding and strain ageing of iron. Proc. Phys. Soc. A 62, 49–62.
Delafosse, D., 2012. Hydrogen effects on the plasticity of face centred cubic (fcc) crystals. In: Gangloff, R.P., Somerday, B.P. (Eds.), Gaseous Hydrogen Embrittlement of Materials in Energy Technologies, vol. 2 . Woodhead Publishing, Cambridge, UK.
Eshelby, J.D., 1954. Distortion of a crystal by point imperfections. J. Appl. Phys. 25, 255–261.
Eshelby, J.D., 1961. Elastic inclusions and inhomogeneities. Prog. Solid Mech. 2, 89–140.
Fleischer, R.L., 1964. Solid-solution hardening. In: Peckner, D. (Ed.), The Strengthening of Metals. Reinhold Publishing Corporation, New York.
Gurtin, M.E., 1972. The Linear Theory of Elasticity, Encyclopedia of Physics, vol. VIa/2. Springer, Berlin.

Haasen, P., 1996. Mechanical properties of solid solutions. In: Cahn, R.W., Haasen, P. (Eds.), Physical Metallurgy4th ed. North-Holland, Amsterdam, The Netherland.
Hirth, J.P., 2013. Private communications.
Hirth, J.P., 1980. Effects of hydrogen on the properties of iron and steel. Metall. Trans. A 11A, 861–890.
Hirth, J.P., Lothe, J., 1968. Theory of Dislocations. McGraw-Hill, New York.
Indenbom, V.L., 1992. Dislocations and internal stresses. In: Indenbom, V.L., Lothe, J. (Eds.), Elastic Strain Fields and Dislocation Mobility. North-Holland, Amsterdam, The Netherlands, pp. 1–174. (Chapter 1).
Khachaturyan, A.G., 1983. Theory of Structural Transformations in Solids. Wiley, New York, p. 488.
Larché, F., Cahn, J.W., 1973. A linear theory of thermochemical equilibrium of solids under stress. Acta Metall. 21, 1051–1063.
Larché, F., Cahn, J.W., 1982. The effect of self-stress on diffusion in solids. Acta Metall. 30, 1835–1845.
Larché, F., Cahn, J.W., 1985. The interactions of composition and stress in crystalline solids. Acta Metall. 30, 331–357.
Louat, N., 1956. The effect of temperature on Cottrell atmospheres. Proc. Phys. Soc. B 69, 459.
Mura, T., 1987. Micromechanics of Defects in Solids, 2nd rev. ed Kluwer Academic Publishers, p. 104, Dordrecht, the Netherlands.
Siems, R., 1970. The influence of correlations on the energy of defect crystals. Phys. Stat. Sol. 42, 105. Eqs. (7–10).
Sofronis, P., 1995. The influence of mobility of dissolved hydrogen on the elastic response of a metal. J. Mech. Phys. Solids 43, 1385–1407.
Sofronis, P., Birnbaum, H.K., 1995. Mechanics of the hydrogen-dislocation-impurity interactions – I. Increasing shear modulus. J. Mech. Phys. Solids 43, 49–90.
Thomson, R., 1958. The nonsaturability of the strain field of a dislocation by point imperfections. Acta Metall. 6, 23.
Wagner, H., Horner, H., 1974. Elastic interaction and the phase transition in coherent metal-hydrogen systems. Adv. Phys. 23, 587. Eq. (5.6).
Wolfer, W.G., Baskes, M.I., 1985. Interstitial solute trapping by edge dislocations. Acta Metall. 33, 2005–2011.